THE CANADIAN JOURNAL OF
CHEMICAL ENGINEERING

Canadian Society for Chemical Engineering | *For Our Future*
Société canadienne de génie chimique | *Pour notre avenir*

An experimental study on the effect of gas injection configuration on flow characteristics in high viscosity oil columns

Shara K. Mohammed[1,2] | Abbas H. Hasan[3] | Abubakr Ibrahim[2] |
Georgios Dimitrakis[2]

[1]Department of Petroleum Technology, Erbil Polytechnic University, Erbil, Iraq

[2]Department of Chemical and Environmental Engineering, Faculty of Engineering, University of Nottingham, Nottingham, UK

[3]Department of Chemical Engineering, Faculty of Science and Engineering, University of Hull, Hull, UK

Correspondence
Shara K. Mohammed, Department of Chemical and Environmental Engineering, Faculty of Engineering, University of Nottingham, Nottingham NG72RD, UK.
Email: shara.mohammed@nottingham.ac.uk

Abstract

Gas-viscous liquid bubbly and slug flow are very common in petroleum, chemical, bioengineering, polymer, and food processing. However, there is a major knowledge gap in two-phase flow research in the design of gas injectors/distributers in very high viscosity oil systems. The present study investigates the effect of gas injection methods in columns containing very high viscosity oils (i.e., realistic liquids), and more specifically using 360 Pa · s viscosity oil in a 240-mm diameter column. The effects that the radial positioning, number of gas nozzles, and their distance from each other have on the structure of the flow in viscous liquids are presented in detail. Electrical capacitance tomography (ECT) is used to extract experimental data. Void fraction, bubble velocity, frequency, liquid film thickness, and bubble length were measured and analyzed at different radial gas injection positions. It has been observed that bubble length increases significantly by 0.3 m when the injection nozzle is located next to the wall of the pipe. Bubble velocity and length also increase by 0.217 m/s and 3.6 m, respectively, with increasing gas flowrate when multiple injection points are used. Increasing the distance between the gas injection points increased bubbles' length by 1.2 m. Bubbles' velocity and frequency (at higher gas flow rate) were also increased.

KEYWORDS
capacitance tomography, large diameter, nozzles, oil gas flow, viscous oils

1 | INTRODUCTION

Gas–liquid flows present a problem of multidimensional complexity due to the infinitely deformable gas–liquid interface and the compressibility of the gas phase. This results in very complex interactions where the kinetic energy is lost in various forms: due to acceleration in the gas phase, turbulence dissipation in the wakes of the bubbles, and friction along the pipe wall.[1] These complex interactions are hugely dependent on the physical properties of the fluids as well as the geometrical parameters (boundary conditions). The extent of the influence of these parameters is not very well established, especially geometrical parameters (injector nozzle, pipe diameter).[2] It is important from a

modelling perspective to establish whether the captured two-phase characteristics are a result of the dynamic interaction of bubbles/structures or hugely dependent on the injection method.[3] If, however the latter is prevalent, it presents an opportunity to exploit with the aim to achieve desired two-phase regimes for various applications. Many operations in the oil and gas industry, chemical processes, and certain natural phenomena such as volcanoes feature liquids that have much lower surface tension than water and much higher viscosity.

Understanding the behaviour of highly viscous fluids is integral to many operations in the oil and gas industry for transport and processing of heavy oils and many refining applications, especially in handling lower distillation products in addition to drilling fluids that can be very viscous. It is also ubiquitous in chemical process industries (CPI) including bioreactors and polymer production like paints, plastic resins, and waxes. Another important relevant industry is the food industry, where there are very viscous liquids like gels, sugar solutions, and chocolate. Viscous fluids handling is also prevalent in the pharmaceutical industry. Moreover, certain natural phenomena such as volcanoes feature very high viscosity magma which is also mirrored in heavy metal moulding applications, including molten eutectic salts. Predicting the behaviour of the flow in high viscosity liquids is essential in order to achieve a safe and efficient design of industrial equipment. The understanding of the possible effects that gas injection methods have on two-phase flow characteristics assists in achieving desired flow regimes for operational purposes (e.g., bubble flow for higher heat/mass transfer). Moreover, investigating the effect of different gas injection configurations on the structure of two-phase flows helps experimentalists to design effective and reliable gas–liquid mixers. Finally, information on gas injection methods is of interest to many modellers who require detailed data regarding the effects of different inlet geometry and boundary conditions on the flow structure during computational studies.

Most of the experimental studies investigating the effect of gas injector geometry on gas–liquid flow use low viscosity liquids (e.g., water). A significantly smaller number of studies focus on viscous fluids in large diameter pipes. One of the earlier studies on the topic is the work of Herringe and Davis,[4] who observed that generally the flow becomes independent of the inlet condition 108D above the mixer point. Conversely, Sekoguchi et al.[5] revealed significant variation in the heat transfer rate due to differences in the void fraction profile generated by different injectors as far as 117D from the injection point. This suggests that the void fraction dependency on inlet condition is likely to be more prominent in smaller diameter flows.

Hills[6] suggested that the flow was not developed when measured at 27D downstream from the injection point, as evidenced by the formation of excessively large bubbles, against expectations for the opposite. Ohnuki and Akimoto[7] reported that the flow structure was dramatically different along the test section. The lower half of the test section (up to 2.1D) near the air injection point showed a specific structure which was affected by the injection method. While the upper part (2.1–4.2D) did not show a considerable effect related to the air injection method according to the phase and the differential pressure distribution in the pipe. In concordance with the study of Hills,[6] wall peaking of the radial void fraction profile was not observed.

Jamialahmadi et al.[8] reported that the bubble size is dependent mainly on the surface tension of the liquid. In addition to the liquid viscosity (which has a considerable effect at high gas flow rates), they have also shown that the bubble size is considerably proportional to the diameter of the nozzle, and it is not affected by the liquid height in the column. A number of studies on the effect of the gas injection nozzle diameter showed a similar result for the strong effect of the nozzle diameter.[9] However, Akita and Yoshida[10] reported that the bubble size is independent of the nozzle diameter.

Hibiki and Ishii[3] reported differences in natural liquid recirculation rates due to injector geometry as well as variations in the flow regime, especially at higher gas superficial velocities as far as 141D downstream the pipe. Similarly, Guet et al.[11] reported that a higher efficiency gas-lift can be achieved by injecting smaller bubbles in a 72-mm vertical pipe air-water system. They also observed that transition to slug flow shifts to higher gas superficial velocity when smaller bubbles are introduced. Lin et al.[12] reported variations in bubble distribution and radial void fraction profiles generated by a sintered and perforated plate injectors in a 230-mm vertical tube measured at 20D.

Similarly, Prasser et al.[13] reported significant variation in the radial profiles of void fraction, gas velocity, and bubble size distribution in a 195-mm vertical pipe when varying the distance between the gas injection and the measuring position between 1.1–40D. Similarly, Omebere-Iyari et al.[14] reported that the flow develops above 7.7D distance, evidenced by the persistence of axial and radial void fraction profiles in addition to bubble size distribution data. This fast development was attributed to the higher gas density ratio, as steam was employed at 65 bar (6500 kPa). However, in their study on a naphtha-nitrogen system, Omebere-Iyari[15] reported some variations as far as a 157D axial distance from the inlet. The long development length was considered an effect of the low viscosity and surface tension of the naphtha.

Kaji et al.[16] found that the void fraction in the Taylor bubble incrementally increases in relation to that in the liquid slug with increasing axial distance. Both Taylor bubbles and liquid slugs length were found to converge around 100D distance.[17] Rabha et al.[18] showed that bubble size grows with increasing axial distance at higher viscosity (0.005 18 Pa · s) in comparison to 0.001 33 Pa · s fluid. The variation was observed between axial distance 4.2D and 13.57D in a 70-mm bubble column. Ibrahim et al.[19] reported that the flow almost converges around 63D downstream from the injection point. It was also reported that longer development length is needed with increasing liquid velocity.

Besagni et al.[20] used two different injectors in a 240-mm large diameter bubble column using liquids of varying viscosities up to 0.007 96 Pa · s. Different void fraction profiles were produced by the two injectors with the fine bubble injector registering higher void fraction overall. The discrepancies seem to diminish with increasing gas superficial velocity. In agreement with the observation of Ibrahim et al.,[21] it was reported that higher viscosity reduces the influence of the inlet geometry. In a recent comprehensive literature review by Besagni et al.,[22] the highest viscosity studied in bubble column applications was quoted as 0.23 Pa · s by Godbole et al.[23] It is worth noting that this viscosity is still well below most of the applications in the food industry and polymer processing. In addition, higher concentration solutions of both materials exhibit highly non-Newtonian behaviour, especially in higher shear zones.

Ibrahim et al.[21] studied the effect of viscosity on flow development in a 127-mm vertical pipe using three different injector geometries and varying the viscosity from 0.005 to 0.105 Pa · s. The flow was reported to develop around 63D axial distance except at low gas superficial velocity. In a recent study by Mohagheghian and Elbing,[24] in a vertical bubble column of diameter ranging between 63–102 mm, it was reported that some variation was observed in the bubble size statistics with changing the diameter and angle of the injector nozzle. This is very expected as the flow is likely not developed considering that the data was captured optically only above 4D axial distance.

From the review on the current studies presented above, it is evident that there is a clear gap in the understanding of the entrance effect in large diameter two-phase flows. It is also apparent that the knowledge gap is rather greater for highly viscous fluids. The present study, therefore, attempts to bridge the knowledge and provide a unique parametric study assessing the influence of a multitude of gas injection geometries on the flow structure in a column of high viscosity oil. The effects of changing the radial position numbers of the gas injection nozzles, the distance between the gas injection points, and the effect of pipe wall on the structure of the flow will be presented. The experiments were conducted using a 240-mm diameter column and silicone oil with a viscosity of 360 Pa · s. Electrical capacitance tomography (ECT) was used to collect information about the characteristics of the flow. Mean void fraction, Taylor bubble velocity and frequency, Taylor bubble and liquid slug lengths, and finally, the liquid film thickness were all determined for the various radial injection positions. Finally, the experimental results have been compared with a selection of empirical models proposed in the literature. In this paper, a review of the previous studies on the effect of gas injection geometry on gas–liquid flow is presented and the gap in this area is identified. The experimental facilities including the rig, fluids, measurements technique, and experimental procedure are presented in detail in Section 2. A comprehensive discussion of the results is presented in Sections 3.1–3.4 corresponding to the type of the experiments. The first section contains a general view for the characteristics of two-phase flow in high viscosity oils. The second section shows the effect of the radial position of a single injection point on the flow structure. The next section explains the effect of the number of nozzles on the flow characteristics by using one versus five nozzles. The last section in the result discusses the effect of the distance between two nozzles. Finally, the conclusions of this work are presented in the last part of this paper.

2 | EXPERIMENTAL SETUP

The current study was conducted at the chemical engineering laboratory in The University of Nottingham. Figure 1 displays the experimental setup which was employed in this work. The experimental rig consists of a column of 0.240-m diameter open to the atmosphere. The column contained silicone oil with an initial height of 3.27 m from the gas injection points. An ECT sensor was installed at 2.5 m from the gas inlet section at the bottom of the column. The gas injection system in Figure 1 consists of two main compressed air lines to obtain a wide range of gas flow rates, high pressure of 95 psi (655 kPa), and low-pressure of 28 psi (193 kPa). The high-pressure line is connected to five flow meters and pressure gauges. Then, each line is divided into five more lines which can be controlled separately by valves (see Figure 1). Thus, the total number of the gas injection lines is 25 lines connected to the bottom section of the columns. The gas flow rate was adjusted and measured using seven flow meters with ranges of 10–50, 50–100, and 100–1500 L/min. The purpose of installing different flow indicators was to obtain a wide range of gas flow rates. A correction equation from the manufacturer was applied to correct the flow rates using the values of the pressure and the temperatures obtained for each flow rate. The rig is also provided with a temperature measurement (thermocouple) to indicate the
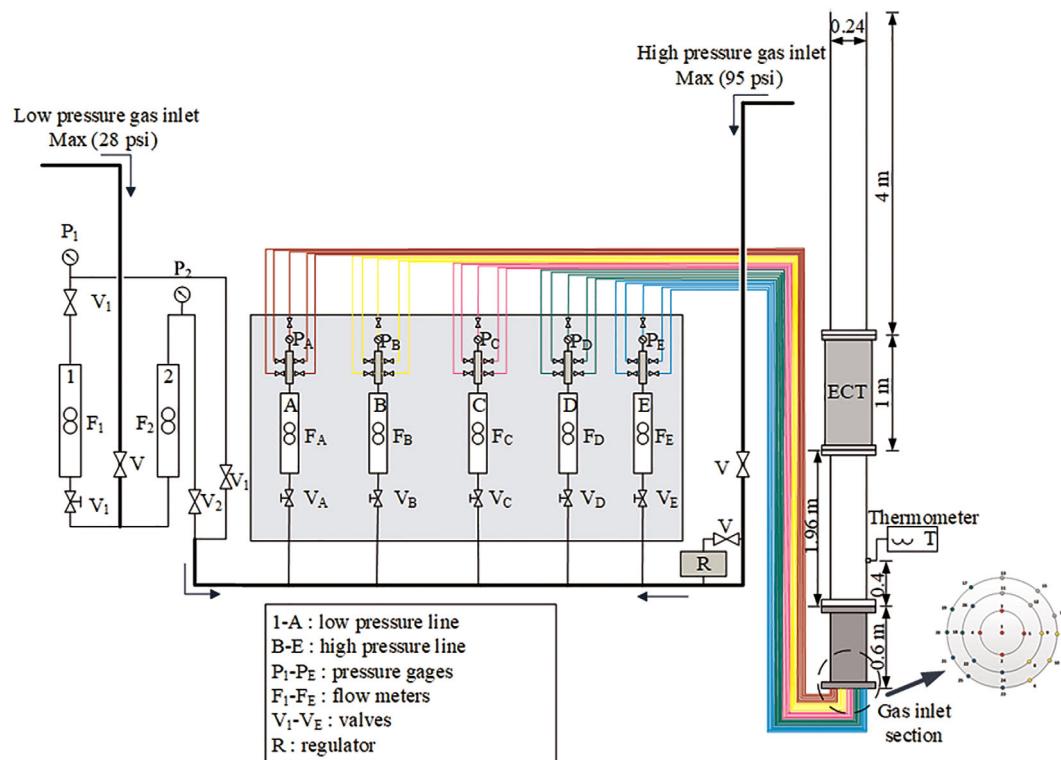
FIGURE 1 Experimental setup employed to investigate the effect of the methods of gas injection in high viscosity liquids[25]

temperature of the air at the gas lines beside the air-oil mixture in the column.

The gas inlet section (see Figure 2) was designed to allow full control of the configuration of the gas flow inside the column by changing the number as well as the position of the gas injection nozzles. The coloured gas lines in Figure 1 correspond to the colours of the gas injection points in Figure 2C. The 25 valves are numbered corresponding to the numbers on the gas inlet section, as is illustrated in Figure 2C. These 25 gas injection points are distributed equally at the bottom of the column. The dashed circular lines represent the three different gas injection rings: they are at 40, 70, and 102 mm from the centre of the pipe cross-section. Figure 2A is a photo of the gas injection section showing the 25 lines connected to the bottom of a 0.240-m diameter column. Figure 2B is a photo of the gas inlet points from inside the column showing the nozzles' distribution.

2.1 | Fluids

In the present work, a high viscosity silicone oil and compressed air were used to study the effect of the gas injection geometry on the flow structure. The oil (XIAMETER PMX-200 Silicone Fluid) was provided by the Dow Chemical Company. The dry air was supplied by two gas

lines from the laboratory compressed air main supply. Detailed information on the fluids used in this work is shown in Table 1.

2.2 | Measurement system

The measurement system used included an ECT sensor, a TFLP-5000 data acquisition box, and a PC for image reconstruction and data processing. The ECT sensor had a 16-electrode configuration, comprising two planes with 36-mm spacing between them.

The dual-plane ECT sensor was installed at 2.5 m from the gas injection, which is equal to 11.27D and 13.6D. This is a sufficient length for which flow development was observed in such viscous oils experimentally. Ibrahim et al.[21] studied the flow development in a 127-mm diameter column using different injector geometries and liquid viscosities (0.004–0.104 Pa · s), they concluded that the flow develops faster with increasing liquid viscosity. This is due to the bubble coalescence rate, which increases significantly with increasing liquid viscosity. Moreover, the equilibrium bubble size occurs faster due to the existence of large bubbles, which develops bubble-induced turbulence on the flow.

ECT is a non-intrusive technique that measures the cross-sectional distribution of capacitance inside the tube,

FIGURE 2 The gas injection section of the 0.24-m diameter column: (A) a photographic image for the lower section of the column connected to 25 tubes, (B) a photographic image of the gas injection nozzles (inside the pipe), and (C) a schematic drawing showing the configuration of the gas nozzles at the bottom of the columns. The colour and the numbers of injection points correspond to the colours and the locations of the tubes in Figure 1
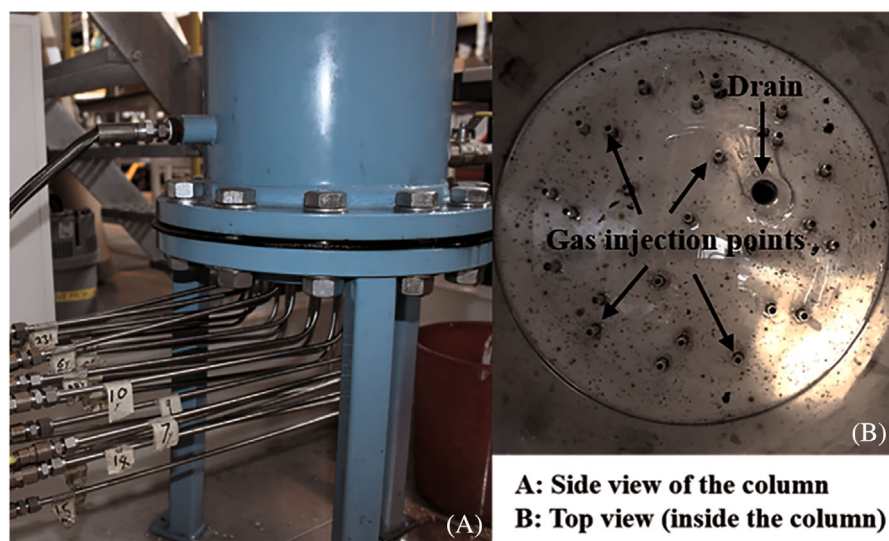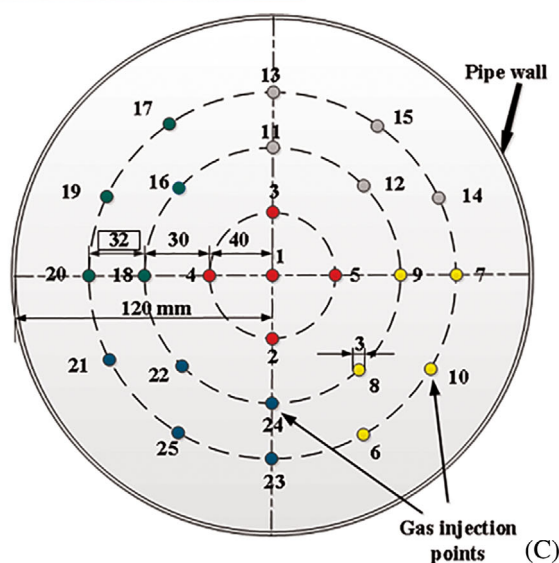
TABLE 1 The properties of the fluids

Fluid (1): Silicon oil				
Column diameter (m)	Viscosity (Pa · s)	Surface tension (N/m)	Density (kg/m^3)	Eötvös number Gρ_lD^2/δ
0.24	360	0.02	950	26 812

Fluid (2): Air				
Gas injection diameter (mm)	Density (kg/m^3)	Temperature (°C)	Low-pressure gas line (kPa)	High-pressure gas line (kPa)
3	1.225	20–23	193	655

which can then be correlated to find the cross-sectional mean phase distribution for non-conductive mixtures. In addition, the structure velocity of the mixture can be determined by cross-correlating the dual sensors of the ECT signals. Azzopardi et al.[26] compared the results obtained from ECT with those obtained from a wire mesh sensor and found good agreement between the two techniques. The validation and uncertainty of the ECT measurements are exhaustively discussed by Mohammed et al.[27]

2.3 | Experimental procedure

In order to investigate the effect of changing the methods of gas injection, three different experiments were conducted. For each run in all the experiments, the data-acquisition time was 600 s and the sampling frequency was 50 Hz (i.e., 30 000 frames per run). The temperature and pressure values during the experiments were also collected and used to establish the correct volumetric flow rate from flowmeters. Table 2 illustrates three different experimental settings in this work. It shows the number of nozzles, the range of gas superficial velocity, the number of runs, and the number of repetitions for each experiment. The experimental procedure is described in Table 2 in more detail.

2.3.1 | Effect of radial/lateral position of a single injection

This experiment was carried out using one gas injection point per run at a constant gas superficial velocity of 0.04 m/s. Seven different positions were used to inject the gas into the bottom of the column and each position was repeated three times. These gas injection points are numbered as 1, 5, 7, 9, 12, 19, and 23, as shown in Figure 2.

2.3.2 | Number of gas injection points

In this experiment, two types of arrangement for the gas injection were used to create the bubbles in both columns. A single-injection point (1), located at the centre of the gas injection section, and five injection points (1, 10, 15, 19, and 25) equally distributed at the bottom of the columns (see Figure 2). For example, the radial distance between point 1 and points 10, 15, 19, and 25 is 102 mm. In addition, the circumferential distance between points 10, 15, 19, and 25 is approximately 53.4 mm. A wide range of gas superficial velocities was applied to obtain different flow regimes. A range of 0.005–0.1 m/s was used for the single nozzle while 0.005–0.063 m/s was used for the five nozzles to obtain the same flow regimes. Each set of experiments was repeated

three times. The aim was to examine the effect of the gas injection points on the flow structure when using more than one gas nozzle.

2.3.3 | Distance between the injection points

This experiment examined the effect of the distance between gas injection points on the flow structure in high viscosity oils. Three different spacings between two gas injection points in parallel were applied. At the same time, the effect of the distance between gas injection points was studied at three different gas flow rates, which created three different flow regimes. These gas injection points were (4 and 5), (9 and 18), and (7 and 20) (i.e., along a diametrical line passing through the centre of the pipe) as shown in Figure 2. In total, three runs with three different gas flow rates and three different spacings between the gas injection points (for each gas flow rate) were used in the experiments and repeated three times. The gas superficial velocities in these experiments were 0.005, 0.01, and 0.1 m/s and a spacing of 80 mm (points 4 and 5), 140 mm (points 9 and 18), and 204 mm (points 7 and 20) was used for each gas superficial velocity.

3 | RESULTS AND DISCUSSION

In this section, comparisons of various flow characteristics are drawn between the current conditions and other relevant work in the literature. It is important to emphasize at this point that caution must be exercised in comparing these results since the physical conditions are very different.

3.1 | Flow characteristics

In the present work, two flow regimes and two types of bubbles were observed over the range of gas flow rates used. The first type includes large spherical bubbles of diameters up to two-thirds of that of the pipe and Taylor bubbles, in bubbly and slug flow regimes. Taylor bubbles in such viscous oil appear with a rounded nose and a

TABLE 2   The conditions and arrangements of the experiments

Experiments	No. of gas injection points	Gas superficial velocities (m/s)	No. of runs/ positions × repetition
Effect of radial/lateral position of a single injection point on the flow structure	1	0.04	7 × 3
Number of injection points	1, 5	(0.005–0.1), (0.005–0.063)	(8 × 3), (10 × 3)
Distance between the injection points	2	0.005, 0.01, 0.1	3 × 3

0.5–2 m long end, having a diameter approximately equal to that of the pipe surrounded by a falling film.[28,29] They are followed by liquid slugs, which fill the space between the large bubbles. The length of the large bubbles (Taylor bubbles) is measured by multiplying the bubble's velocity and the time each bubble takes to rise through the ECT planes. The second type consists of smaller bubbles (daughter bubbles by Bird et al.[30]) of two different diameters. One in the order of centimetres (the shapes vary between ellipsoidal and spherical) and the other having a diameter of a few millimetres and being spherical in shape. They are usually distributed in the liquid slug and the falling film. Figure 3 shows the large bubbles in bubbly and slug flow regimes accompanied by the small bubbles encountered in the flow. In this paper, the focus will be mainly on the features and characteristics of large bubbles in the column. The term large bubble is used for the large spherical bubbles in the bubbly and slug flow regimes, while Taylor bubble is used for the elongated cylindrical bubbles in the slug flow regime. Increasing bubble length/size manifests as an increase in the diameter of the spherical bubbles and the length of the Taylor bubbles. It is worth noting that, in the case of the different sizes of bubbles encountered in this study, the turbulence that usually occurs in the wake of bubbles is observed to be minimal. This is very clearly noticeable in the absence of the cap-shaped bubbles or bullet-shaped Taylor bubbles where the falling liquid film around the faster-rising bubbles would meet the liquid bulk, creating turbulent eddies in their wake. As is plainly evident in Figure 3, these falling film eddies are greatly dampened by the viscous forces, resulting in a smooth, rounded tail of the bubbles with limited entrapment of daughter bubbles in their wakes.
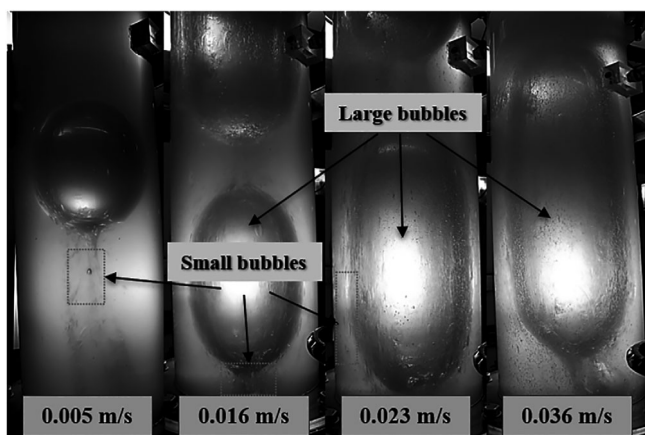
Figure 4 shows time-resolved tomographic images of the cross-sectional phase distribution produced by the ECT featuring the three characteristic flow regimes captured in Figure 3. Furthermore, instances of coalescence between bubbles in the various regimes are also captured. It can also be seen that, due to the ill-posed nature of the phase reconstruction problem, the smaller bubbles trapped in the liquid bulk are not resolved but rather represented as regions of faded red colour in the liquid. Increasing the gas superficial velocity leads to more bubble coalescence as can be seen in Figure 3 at 0.023 m/s. This can be attributed to the fact that as the gas superficial velocity increases the bubble velocity increases. In addition, the burst of these bubbles at the top of the column followed by a falling of the liquid film entrapping gas bubbles and the retracting of the liquid film led to an increase in the chance of bubble coalescence. [29]

3.2 | Effect of radial/lateral position of a single injection point on the flow structure

The effect of a single gas injection position on the characteristics of slug flow regime in viscous liquids in a
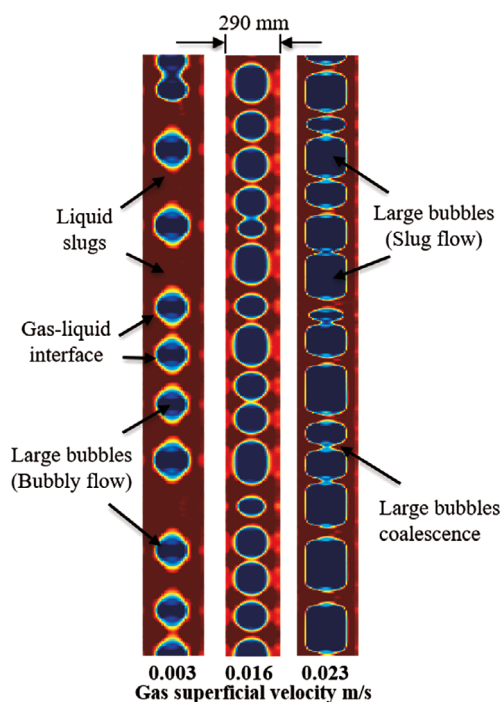

FIGURE 3 A photograph showing the structure of the flow in a 360 Pa · s silicone oil and 240-mm diameter column at 0.005, 0.016, 0.023, and 0.036 m/s gas superficial velocities. The marked areas show the small bubbles flow at the wakes of the large bubbles and at the falling liquid film around the large bubbles

FIGURE 4 Electrical capacitance tomography (ECT) images of gas–liquid flow at different velocities: gas represented in blue, liquid in red, and mixed hues for the interface. The reconstructed images are for a 290-mm diameter column of 330 Pa · s silicone oil at gas superficial velocities of 0.003, 0.016, and 0.023 m/s. The images are sets of multiple 2D image frames as 2D slices (10 000 frames)[28]

240-mm diameter column was investigated at a gas superficial velocity of 0.04 m/s This gas superficial velocity is selected as it can generate a series of clear ellipsoidal bubbles (i.e., a fully developed slug flow), which fits well with the scope of the current study, allowing for the investigation of the effect of gas injection position on the flow features of slug flows.

The time series of the void fraction obtained from the ECT can be used to infer the behaviour of Taylor bubbles for each of the studied cases. Figure 5 shows the time series of the cross-sectional averaged void fraction of the flow using one gas injection point each time/run. The first time series (at the top) is when the nozzle at the centre of the gas injection section is used. The second one corresponds to the flow when only the nozzle at 40-mm distance from the centre is used. Similarly, the third and the fourth time series in the figure are when using the nozzles at 70- and 102-mm distance from the centre, respectively. Void fraction in Figure 5 shows no significant dependency on changing the position of the nozzles. In other words, the mean void fractions at different injection positions are approximately the same (i.e., 0.381).

However, the flow structure shows some variation with the change of gas injection position. The bubbles seem consistent/coherent for all positions of the nozzles. It also seems that the bubbles, using the central gas injection nozzle, are more uniform. The rate of coalescence between the bubbles is slightly increased with changing the position of the nozzle towards the pipe wall. At the 102-mm injection distance from the centre, the bubbles appear to vary in length due to the increasing rate of coalescence. The bubbles become longer when nozzles are closer to the pipe wall. This might be due to wall effects, where the no-slip condition at the wall results in a higher shear stress region in the gas/liquid interface closest to the wall This, in turn, could produce a reduced drag region that would encourage bubble coalescence.[31]

Figure 6 shows the effect of changing the position of gas injection points on the cross sectional and time-averaged void fraction in 240-mm diameter columns. The first and second positions, which are at the centre and 40-mm distance from the centre (nozzle 5 in Figure 2C), represent one nozzle and one position. However, the injection points at 70 and 102 mm are used at different locations at the same circle. For example, the 70-mm radius circle contains 8 nozzles; only nozzles 9 and 12 are used (separately) in this case. Similarly, in the 102-mm radius circle, which contains 12 nozzles equally distributed, nozzles 7, 19, and 23 are used for gas injection one at a time.

The averaged void fraction presented in Figure 6 shows no significant change as a consequence of changing the position of the gas injection nozzles. However, the average void fraction seems slightly higher near the pipe wall in comparison with the pipe centre. Injecting gas near the wall improves bubble coalescence, resulting in longer and slightly faster rising bubbles registering the higher average void fraction. Standard error, which was calculated from the standard deviation divided by the square root of the number of the repeated values, was around 0.1%.
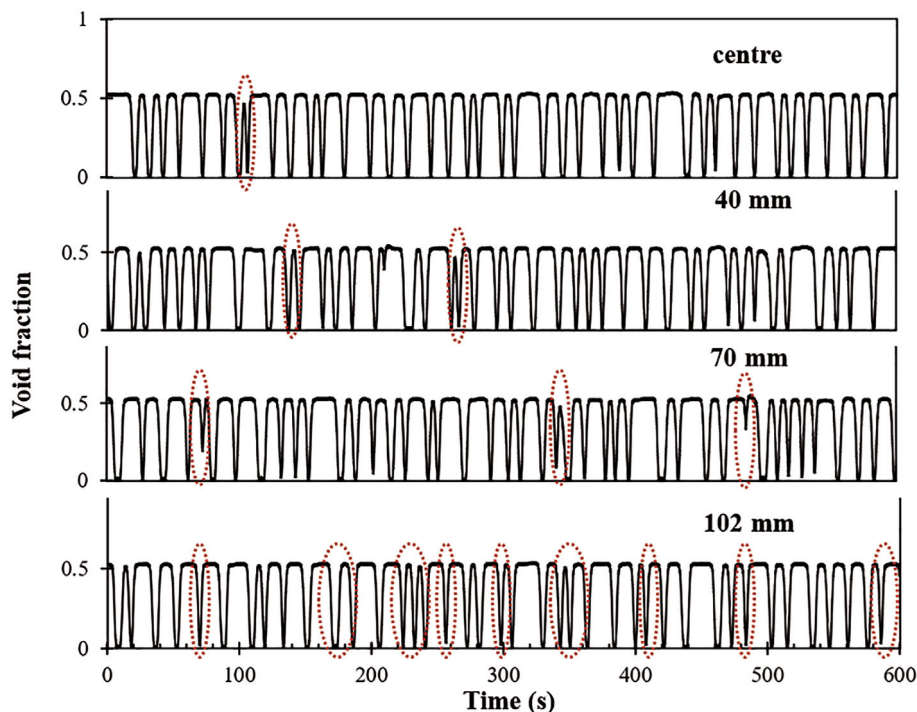

FIGURE 5 The effect of the radial position of a single gas injection point on the time series of the cross-sectional averaged void fraction in 360 Pa · s silicone oil, 240-mm diameter column, and 0.04 m/s gas superficial velocity. The gas injection points locations are at the pipe centre, 40, 70, and 102 mm from the pipe centre. The marked areas show the bubble coalescence along the column
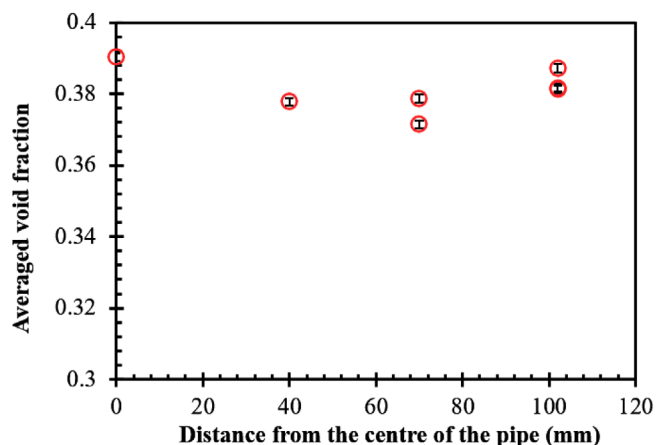
MOHAMMED ET AL.

THE CANADIAN JOURNAL OF
CHEMICAL ENGINEERING

Canadian Society for Chemical Engineering | *For Our Future.*
Société canadienne de génie chimique | *Pour notre avenir*

9

FIGURE 6 Evolution of cross-sectionally and time-averaged void fraction with the positioning of the gas injection nozzle at the base of the column is shown. The figure presents time averaged void fraction of slug flow regime in 360 Pa · s viscosity silicone oil using a single nozzle at different positions in a 240-mm diameter column at 0.04 m/s gas superficial velocity

Figure 7A–D shows the effect of changing the position of a single gas injection point on Taylor bubble velocity, Taylor bubble length, frequency, and film thickness, respectively, at a constant gas flowrate. Likewise, the bubbles' velocity in Figure 7A did not show a significant dependency on changing the positions of the gas injection points. The velocity of the Taylor bubbles was calculated from the cross-correlation of the void fraction signals extracted from the two ECT planes. The time delay between the signals of the planes was used in conjunction with the distance between the planes to calculate the bubble velocity (velocity being equal length divided by time). Taylor bubble velocity increased slightly by 0.0007 m/s by changing the nozzle location from the centre to the pipe wall. This corresponds to increasing the coalescence between the bubbles creating larger/longer bubbles: 'Larger bubbles rise faster because of the balance between the buoyant weight and the drag force'.[33]

Taylor bubble velocity, $U_{tb} = Fr\sqrt{(gD)}$, was determined theoretically and experimentally by Davies and Taylor[34] and Nicklin.[35] Viana et al.[36] presented an equation to determine the value of Froude number, Fr, basing on the buoyancy Reynolds number and Eötvös number. A universal correlation for two regions separated by a transition region (10 < R < 200) was also presented by Viana et al.[36] The two regions consist of an inclined region of low buoyancy Reynolds number and a flat region of high buoyancy Reynolds number. Azzopardi et al.[37] used liquids with different viscosities (up to 360 Pa · s) and showed accurate values of Fr. The rise velocity of the isolated Taylor bubble, U_{tb}, in a turbulent flowing liquid can be determined by the following relationship[35]:

$$U_{tb} = C_o\left(U_{gs} + U_{ls}\right) + K\,Fr\sqrt{gD} \tag{1}$$

where the coefficient C_o represents the ratio of the centreline to cross-sectionally average velocities, which is equal to 1.2; U_{gs} and U_{ls} are the gas and liquid superficial velocities, respectively; $K = 0.905/(1\text{-}\alpha s)^{3.95}$, where αs is the void fraction in the liquid slug part of the flow; Fr is Froude number; g is gravitational acceleration; and D is pipe diameter.

A minor modification based on a strong theoretical support was proposed by Collins et al.[38] for Equation (1) by Nicklin,[35] suggesting $C_o = 1.29$. The difference in the pipe's diameter is the reason of the different values of C_o. Nevertheless, the higher values of C_o are more suitable for the lower flow rates.[35] A more complicated relationship to calculate C_o value was suggested by Dukler and Fabre[39] and Guet et al.,[40] which is given by the following:

$$C_o = \frac{C_{Bc}}{\left[1 + \left(\frac{Rem}{Rec}\right)^2\right]} + \frac{C_{0,Re=\infty}}{\left[1 + \left(\frac{Rec}{Rem}\right)^2\right]} \tag{2}$$

where C_{Bc} is the distribution parameter for zero liquid input slug flow = 2.27, R_{ec} is the critical Reynolds number = 4000, $C_{0,Re=\infty}$ is the distribution parameter of large input slug flow = 1.2, and R_{em} is the mixture Reynolds number = $[D\,\rho_l(U_{gs} + U_{ls})]/\mu_l$.

When compared with the analytical method proposed by Viana et al.,[36] the ECT results showed a maximum relative deviation of 2% (see Figure 7A).

The length of Taylor bubbles was calculated using the threshold by relating the time of Taylor bubble obtained from the time series with the structure velocity obtained from the cross-correlation of the void fraction signals from the ECT planes. As can be seen from Figure 7B, the Taylor bubble length is significantly affected by the radial position of the gas injection nozzles; it increased by 0.3 m when the position of the nozzles moved from the centre towards the pipe wall. This also confirms the finding observed from the time series of the void fraction (see Figure 5), in which more coalescence occurred when the gas injection point moved towards the pipe wall, causing an increase in bubbles' length. The no-slip condition at the pipe wall may lead to a higher shear stress in the gas/liquid interface which could increase the chance of bubble coalescence, leading to increase in the length of the bubbles. Experimental bubble length was compared with the approach of Khatib and Richardson,[32] who
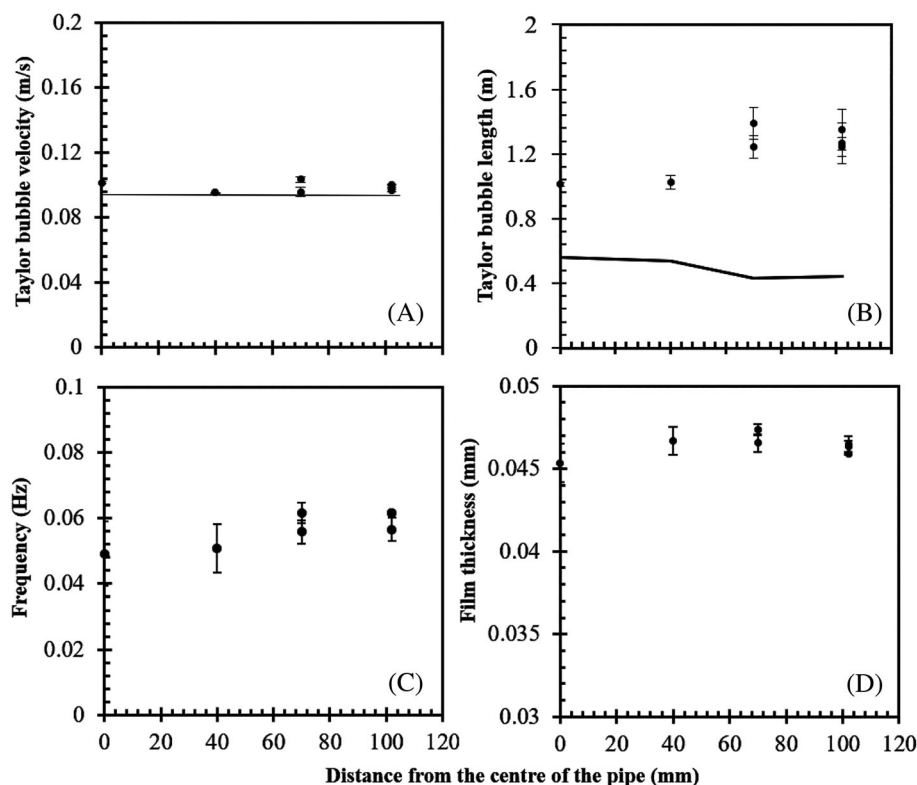
FIGURE 7 Taylor bubbles' two-phase flow characteristics with varying the location of a single injection nozzle from the centre of the column: (A) Taylor bubble rise velocity in a 240-mm diameter column of 360 Pa · s viscosity silicone oil, ● from electrical capacitance tomography (ECT), — calculated from Equation (1), $C_{Bc} = 2.27$; (B) experimental and analytical lengths of Taylor bubble, ● Taylor bubble (ECT), — Taylor bubble[32]; (C) frequency of Taylor bubbles rising in the column; and (D) liquid film thickness around large bubbles. In (A–D) a single gas injection point at different positions is used at 0.04 m/s gas superficial velocity. The standard error is calculated from the standard deviation and the square root of the number of repeated values

proposed an equation to calculate the length of the Taylor bubble numerically. In their equation, they used the values of the probability density function (PDF) averaged void fraction to calculate the Taylor bubble and liquid slug length, L_{TB} and L_S, respectively. The length of the slug unit L_u can be calculated from the structure velocity U_{st} (from cross-correlation of the two planes of the ECT) and the frequency f of the Taylor bubble, that is, $L_u = U_{st}/f$, where $L_u = L_S + L_{TB}$. Therefore, $L_S/L_u = (\alpha - \alpha_{TB})/(\alpha_s - \alpha_{TB})$. α is the overall void fraction, α_{TB} is the void fraction of Taylor bubble (a void fraction which is corresponding to the higher PDF peak value), and α_S is the void fraction of liquid slug (corresponding to the lower PDF peak value).

In general, the analytical results calculated from the approach proposed by Khatib and Richardson[32] show no considerable change with moving the gas injection points.

The frequency of Taylor bubbles was calculated by means of counting the number of individual bubbles per unit time. The frequency of Taylor bubbles was increased by 0.01 Hz by moving the gas injection point towards the pipe wall (see Figure 7C).

Another parameter, which also does not show a significant variation with change in the injection position, is the film thickness, which is determined by the geometric relationship $\delta = (D/2)(1 - \sqrt{\varepsilon_g})$ as displayed in Figure 7D.

3.3 | Number of injection points

The effect that the arrangement of the gas injection points has on the bubble formation in a 240-mm diameter column was investigated by employing two different configurations. A single injection point, which was located in the centre of the gas injection section, and five injection points distributed equally at the bottom of the columns (i.e., the central nozzle 1 and the four nozzles closest to the pipe wall: nozzles 10, 15, 19, and 25; see Figure 2). The aim is to examine the effect of the coalescence between the bubbles at the gas injection points on the flow structure when using more than one gas injection.

For the range of flow rates used, two flow patterns were mainly observed in the column: bubbly and slug flow. The time series of cross-sectional averaged void fractions obtained from the ECT show the difference in the behaviour of the flow when using single or multiple injection points. Figure 8 illustrates the time series of cross-sectional void fraction in the 240-mm diameter column for two types of gas injection settings (a single centred injection point and five injection points, see Figure 2) at different gas flow rates. In both injection settings, bubble length/size increased with an increasing gas flowrate, which resulted in an increasing bubble velocity.[33]

In bubbly flow (with a gas superficial velocity, 0.005 m/s), it appears that the number of bubbles (and hence the frequency), using only a central nozzle, is
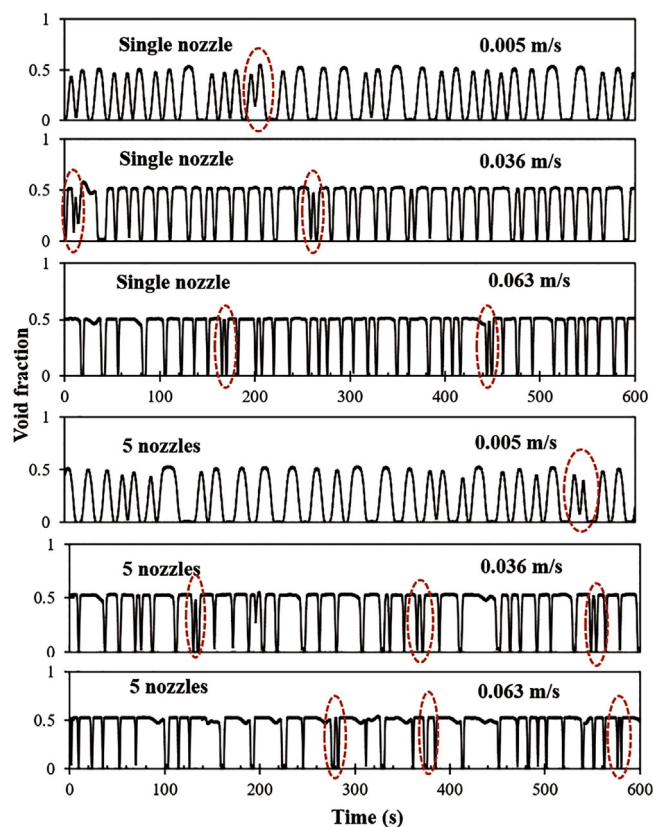
FIGURE 8 Single versus multiple gas injection nozzles effect on cross-sectionally averaged void fraction time series and instances of bubbles' coalescence. Comparing the time series of the cross-sectional averaged void fraction of gas flow in 360 Pa · s silicone oil for single gas injection point (centre) with five injection points (1, 3, 15, 19, and 25) in a 240-mm diameter column. The marked areas represent bubble coalescence

FIGURE 9 Single versus multiple nozzles effect on two-phase mixing with increasing gas superficial velocity. Comparing the effect of gas superficial velocity on the time-averaged void fraction for a single nozzle at the centre of the gas injection section and five nozzles distributed equally at the injection section at the bottom of a 240-mm diameter column of viscous oil. Maximum standard errors are 0.1% and 0.11% for the single and multiple nozzles, respectively

higher than that when using five gas injection nozzles. In addition, the individual bubbles are quite a bit bigger in the case of the five-nozzle configuration. This can be explained by considering the mechanics of bubble initiation and detachment during the injection. When multiple nozzles are used, initially smaller bubbles are introduced with very small terminal velocities. They grow in size at the injection zone until the buoyancy dominates where they start rising, while migrating to the centre of the pipe, hence coalescing to form bigger and longer bubbles.[26] At gas superficial velocities of 0.036 and 0.063 m/s (i.e., slug flow), the Taylor bubbles (using five gas injection nozzles) are longer than those when using one central nozzle due to the bubble coalescence.

Figure 9 shows the effect of increasing the gas superficial velocity on the averaged void fraction using one gas injection point at the centre of the gas injection section. It also shows the effect of changing the gas superficial velocity of the averaged void fraction using five gas nozzles. Finally, it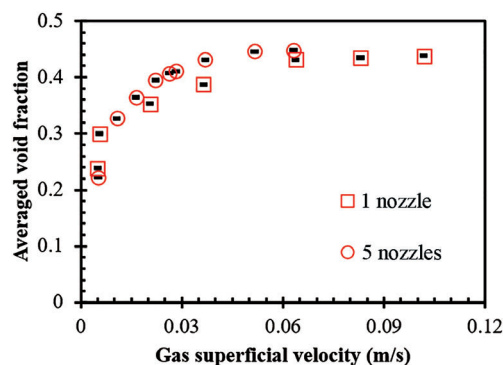 compares both gas injection arrangements for a wide range of gas flow rates. As expected, the average void fraction increases with increasing gas flow rates.[37]

The average void fraction is higher by 0.1 when using five gas injection points. This is also expected as the bubbles are slightly longer. The standard deviation of the average void fraction is calculated for all flowrates. It can be observed that the void fraction in slug flow is almost independent of the gas superficial velocity. This could be due to the very long bubbles which appear as an open core at a high range of gas flow rates. The nose of the bubble bursts at the top of the column while the bubble bottom still attaches to the gas nozzles and appears as a gas column in the centre of the pipe surrounded by a falling liquid film on the wall. This mechanism was investigated in more detail by Mohammed et al.[27]

Figure 10A–D shows the effect of increasing gas superficial velocity on Taylor bubble velocity, Taylor bubble length, frequency, and film thickness, respectively, using two gas injection configurations (1 or 5 s). The rise velocity of the bubbles, which is illustrated in Figure 10A, increases with an increasing gas flow rate for both gas injection arrangements. Bubble velocity values appear higher when using five gas injection points; corresponding to the larger bubble size, they increase with increasing bubble size/length.[41] Two different line slopes can be found in Figure 10A. This corresponds to the flow regime transition from bubbly to slug flows. The rise velocity of the bubbles, which is illustrated in Figure 10A, increases with an increasing gas flow rate for both gas injection arrangements. Bubble velocity values appear higher when using five gas injection points corresponding to the larger bubble size; they increase with increasing bubble size/length.[41]
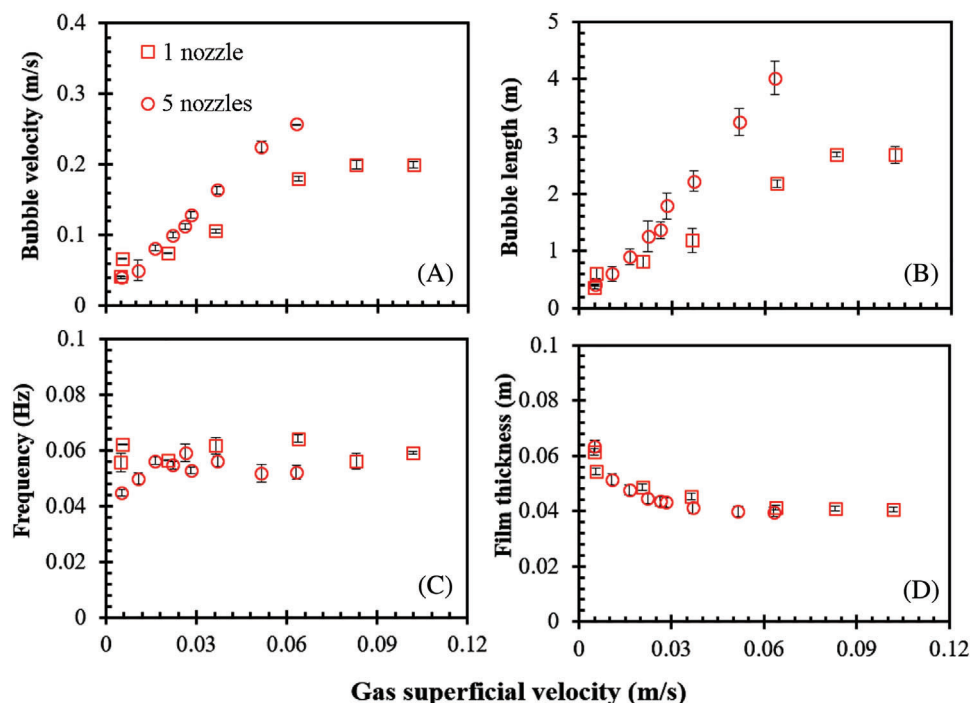
FIGURE 10 Single versus multiple gas nozzles effect on two-phase mixing with increasing gas superficial velocity: (A) bubbles rise velocity, (B) bubbles length, (C) bubbles frequency, and (D) liquid film thickness around large bubbles. The bubbles are rising in 360 Pa · s silicone oil and a 240-mm diameter column. The standard error is calculated from the standard deviation and the square root of the number of repeated values

The average length of the Taylor bubble L_{tb} can be determined by multiplying the structure velocity (obtained from a dual-plane ECT) and the average passing time of the Taylor bubbles (extracted from the void fraction time series). Figure 10B shows that bubble length increases with an increasing gas flowrate for both gas injection settings. Bubble length using five gas injection points is greater than that using a single gas injection point, particularly at moderate to high gas superficial velocity. This is due to the rate of the coalescence, which appears higher when using five injection points, as these injection points are closest to the pipe wall.

The average length of the bubbles was observed to increase up to 1.8 m in the case of a single gas nozzle, while it increases significantly up to 3.6 m when using five nozzles for the same range of gas flow rates. Therefore, the growth rate of the bubble's length is higher when five injection nozzles are used. This can be further investigated to find the optimum configuration to control the size of the bubbles inside the column/pipelines for the efficient and safe design of equipment.

Generally, bubble frequency appears to decrease slightly with increasing the gas flowrate in both gas injection arrangements (see Figure 10C). The frequency of the bubbles increases when using a single gas injection nozzle from 0.056 to 0.059 Hz for gas superficial velocities of 0.005–0.1 m/s. Bubble frequency increased from 0.04 to 0.05 Hz when using five gas injection nozzles for gas superficial velocities of 0.005–0.06 m/s. This is due to the higher coalescence rate, which creates longer bubbles when using five gas injection points. The increased bubble frequency could

be related to the rise of bubble velocity, which is balanced by the growth in the bubble's length. At higher gas flow rate, bubbles' frequency is approximately independent of the gas flow rates due to the uniform Taylor bubbles that occupied almost the entire diameter of the column and move quite uniformly upwards.[42]

Figure 10D illustrates the film thickness around the large bubbles, which is calculated from the mean void fraction. Generally, the values of film thickness decrease with increasing gas flow rates in all cases. This is due to an increase in the size/diameter of bubbles with increasing gas flow rates. In other words, for bubbly flow, as the bubbles grow, their film thickness decreases. At higher gas flowrates (i.e., slug flow), the film thickness seems to be independent of the gas flow rate. The same finding was also reported by Azzopardi et al.[37] This can be attributed to the fact that Taylor bubbles grow to occupy almost the entire cross-section of the pipe; any increase in gas flow-rate contributes to the growth of bubble length and not its diameter. Comparing the effects of changing the number of gas injection points on the film thickness, no significant change is observed. Film thickness is slightly lower when using multiple gas injection points as the diameter of the bubbles is slightly larger when five nozzles are used.

3.4 | Distance between the injection points

In order to determine the effect that the space between the gas injection points has on the structure of flow in

high viscosity liquids, two simultaneous gas injection points were used at the bottom of the column, and the distance between the injection points was changed for each run. In total, three different gas flow rates (0.005, 0.01, and 0.1 m/s) and three different spacings between the gas injection points (for each gas flow rate) were used in the experiments and repeated three times.

In general, mean void fraction, bubble velocity, film thickness, and bubble frequency do not show any significant variation. In contrast, the Taylor bubble length was observed to change. Figure 11 shows the effect of changing the spacing between two gas injection points on the averaged void fraction at three different gas flow rates. In addition, it shows the effect of changing the space between three gas injection points on the liquid film thickness around Taylor bubbles using the same gas flow rates. The results show that, at the fixed gas flow rate, void fraction and film thickness are not affected by increasing distance between the injection points, although a slight increase is shown at a higher gas flow rate (0.1 m/s). However, increasing the distance between the gas injection points appears to affect the length of the bubbles, bubble velocity, and frequency. As can be seen in Figure 12A, bubble length increases significantly by 1.2 m with increasing distance between the two gas injection points by 124 mm at the higher gas flow. Standard
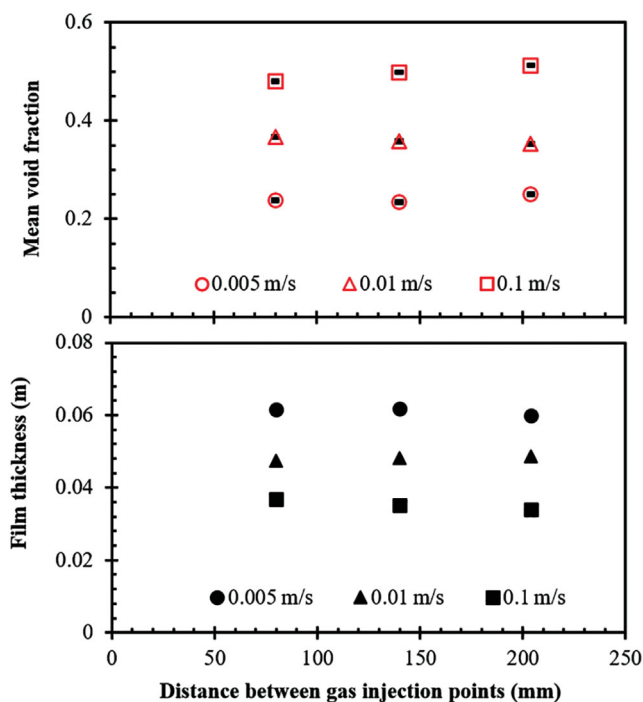
errors were calculated from the standard deviation and the square root of the number of repeated values. They were around 0.12%, 0.13%, and 0.1% at gas superficial velocities of 0.005, 0.01, and 0.1 m/s, respectively.

On the other hand, bubbles' length at lower gas superficial velocities (i.e., 0.005 and 0.01 m/s) seems to be independent of gas injection positions (see Figure 12A). However, at high gas flow (0.1 m/s) there is a significant increase (from 2 to 3.2 m) in the length of the bubble with changing gas injection points. This is synonymous with the increased rate of bubble coalescence observed when five nozzles are used in comparison to a single nozzle, as discussed earlier.

Figure 12B shows the variation of the mean bubble velocity at different gas injection combinations. Bubble velocity becomes sensitive to the gas injection position at higher gas flow rates while at low gas flow rates it is seen that there are no significant changes. Bubble velocity
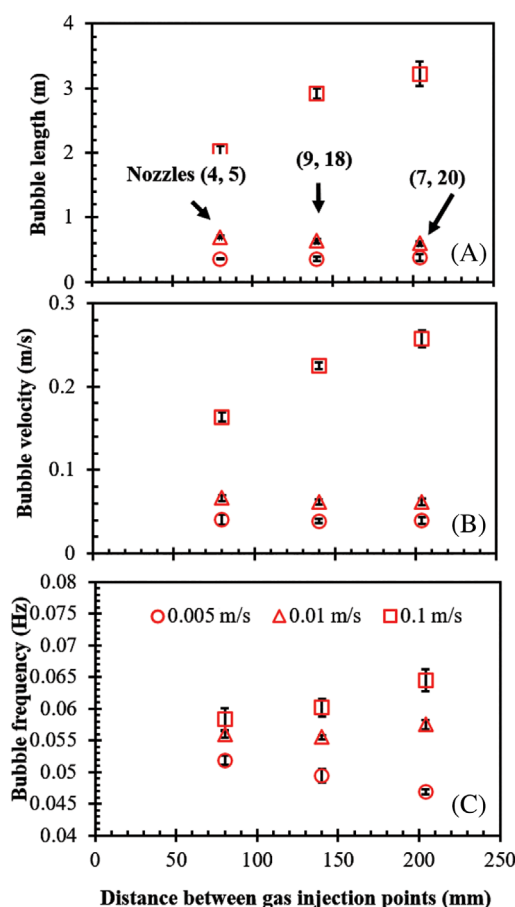

FIGURE 11 The effect of increasing the distance between two gas injection points on mean void fraction and liquid film thickness in high viscosity oil and a 240-mm diameter column using different gas superficial velocities. Standard errors are 0.12%, 0.13%, and 0.1% at gas superficial velocities of 0.005, 0.01, and 0.1 m/s, respectively

FIGURE 12 The effect of increasing the distance between two gas injection points on the flow structure in high viscosity oil and a 240-mm diameter column using different gas superficial velocities (0.005, 0.01, 0.1 m/s): (A) bubble length, (B) bubble rise velocity, and (C) bubble frequency. The standard error is calculated from the standard deviation and the square root of the number of repeated values

increases by 0.094 m/s as the distance between both gas injection points increases by 124 mm at the higher gas flowrate. This increase in bubble velocity corresponds to the increase in bubble length/size, as larger bubbles rise faster,[33] while at lower gas flowrates, bubble velocity seems constant due to the drag force. In high viscosity liquids, for smaller bubbles drag force is more dominant; a slight increase in bubble size at low gas velocities would result in a negligible rise in bubble velocity. When the size of the bubble is smaller, the surface area/volume ratio is very high, which means the drag force dominates the bubble dynamics. This increase in the bubble velocity (i.e., at a higher gas flow rate in slug flow) could also lead to an increase in the frequency of the Taylor bubble as shown in Figure 12C. At lower gas superficial velocities, when increasing the distance between injection points, smaller bubbles are generated. As a result, bubble velocity decreases and therefore, frequency decreases. As gas superficial velocity increases, the separated nozzle improves bubble coalescence, leading to larger bubbles and therefore higher rise velocity and higher frequency. Similar to the observed behaviour of five nozzles in comparison to the one central nozzle addressed earlier. It should be noted that the bubble size needs to increase beyond a particular critical value when buoyancy overcomes drag, where the increase in gas flowrate is manifested in increased bubble rise velocity, and hence, frequency.

4 | CONCLUSIONS

Starting with the radial position of a single injection point, Taylor bubble velocity increases slightly by 0.0007 m/s when diverting a single injection nozzle from the centre towards the pipe wall by 102 mm. This is most likely due to the lateral migration of bubbles away from the high shear region near the wall to the centre, thus increasing the rate of coalescence, leading to the formation of large/long bubbles that move faster in the column. Bubbles' length is significantly affected by the radial position of the gas injection nozzles; it increases substantially by 0.3 m when the gas injection points move from the centre towards the pipe wall. Bubble frequency increases by 0.01 Hz by moving the gas injector from the centre to the pipe wall. The liquid film thickness is not significantly affected by moving a single gas injection position from the centre towards the pipe wall.

The use of five gas injection points causes both bubbles' velocity and bubbles' length to significantly increase by 0.217 m/s and 3.6 m, respectively for an increase in the gas flow rate from 0.005 to 0.1 m/s. Using a single gas injector, bubbles' velocity and length increase by 0.14 m/s and 1.8 m, respectively, with increasing gas flow rate. Bubbles' frequency increases by 0.008 and 0.01 Hz when using a single and five gas nozzles, respectively, with increasing gas flow rate. Liquid film thickness is independent of the gas superficial velocity for both gas injection configurations. The average void fraction is higher by 0.1 when using five gas nozzles.

Finally, increasing the distance between the injection points increases the length, velocity, and frequency of the bubbles significantly at high gas flow rates. Bubble velocity and length increase by 0.094 m/s and 1.2 m, respectively, as the distance between the two gas nozzles increases by 124 mm. This increase in bubble velocity corresponds to the increase in bubble length/size, as larger bubbles rise faster, and increases bubbles frequency. At lower gas flowrates, by increasing the distance between two injection points, smaller bubbles generate with a lower rise velocity, which leads to lower bubble frequency.

Dedication
This work is dedicated to the memory of Professor Barry J. Azzopardi a project leader and good friend. The new findings in this work could not have been achieved without his knowledge, guidance, and support.

AUTHOR CONTRIBUTIONS
Shara K Mohammed: Conceptualization; data curation; formal analysis; funding acquisition; investigation; methodology; resources; software; visualization; writing – original draft; writing – review and editing. **Abbas H Hasan:** Supervision; writing – review and editing. **Abubakr Ibrahim:** Writing – review and editing. **Georgios Dimitrakis:** Supervision; writing – review and editing.

PEER REVIEW
The peer review history for this article is available at https://publons.com/publon/10.1002/cjce.24312.

NOMENCLATURE

C_{Bc}	distribution parameter for zero liquid input slug flow = 2.27[37]
C_o	ratio of the centreline to cross-sectionally average velocities
$C_{0,Re=\infty}$	distribution parameter of large input slug flow = 1.2[38,39]
D	pipe diameter (m)
E_o	Eötvös number, ratio of the interfacial tension and viscous forces, $E_o = (g\,\rho_l D^2)/\sigma$

MOHAMMED ET AL.

THE CANADIAN JOURNAL OF CHEMICAL ENGINEERING

Canadian Society for Chemical Engineering | *For Our Future.*
Société canadienne de génie chimique | *Pour notre avenir*

15

F_r	Froude number, dimensionless velocity, ratio of the gravitational and inertial forces $= 0.351$ or 0.328
g	gravitational acceleration (m/s^2)
K	$= 0.905/(1 - \alpha_s)^{3.95}$[34]
L_u	length of slug unit (m)
L_{TB}	length of Taylor bubble (m)
L_s	length of liquid slug (m)
R	Buoyancy Reynolds number, dimensionless inverse velocity $R = \sqrt{[D^3 g(\rho_l - \rho_g)\rho_l]/\mu)}$
R_{em}	mixture Reynolds number, $D\rho_l(U_{gs} + U_{ls})]/\mu$
R_{ec}	critical Reynolds number $= 4000$[39]
U_{tb}	Taylor bubble velocity (m/s)
U_{gs}	gas superficial velocity (m/s)
U_{ls}	liquid superficial velocity (m/s)
U_{st}	structure velocity (m/s)

Greek symbols

α	overall void fraction
α_s	void fraction of liquid slug
α_{TB}	void fraction of Taylor bubble
δ	liquid film thickness (m)
ε_g	void fraction from the ECT
μ	liquid viscosity (Pa · s)
ρ_l	liquid density (kg/m^3)
ρ_g	gas density (kg/m^3)
σ	surface tension (N/m)

ORCID

Shara K. Mohammed https://orcid.org/0000-0002-4804-6230

REFERENCES

[1] M. Iguchi, O. Ilegbusi, *Modeling Multiphase Materials Processes Gas-Liquid Systems*, Springer, New York **2011**, p. 1.

[2] M. Ishii, T. Hibiki, *Thermo-Fluid Dynamics of Two-Phase Flow*, 2nd ed., Springer Science & Business Media, New York **2011**.

[3] T. Hibiki, M. Ishii, *Nucl. Eng. Des.* **2001**, *203*, 209.

[4] R. Herringe, M. Davis, *J. Fluid Mech.* **1976**, *73*, 97.

[5] K. Sekoguchi, M. Nakazatomi, Y. Sato, O. Tanaka, *B. JSME* **1980**, *23*, 1625.

[6] J. Hills, *Chem. Eng. J. Bioch. Eng.* **1993**, *53*, 115.

[7] A. Ohnuki, H. Akimoto, *Int. J. Multiphas. Flow* **1996**, *22*, 1143.

[8] M. Jamialahmadi, M. Zehtaban, H. Müller-Steinhagen, A. Sarraf, J. Smith, *Chem. Eng. Res. Des.* **2001**, *79*, 523.

[9] A. Kumar, T. E. Degaleesan, G. S. Laddha, H. E. Hoelscher, *Can. J. Chem. Eng.* **1976**, *54*, 503.

[10] K. Akita, F. Yoshida, *Ind. Eng. Chem. Proc. D.D.* **1974**, *13*, 84.

[11] S. Guet, G. Ooms, R. Oliemans, R. Mudde, *AIChE J.* **2003**, *49*, 2242.

[12] J. Lin, M. Han, T. Wang, T. Zhang, J. Wang, Y. Jin, *Chem. Eng. J.* **2004**, *102*, 51.

[13] H. M. Prasser, M. Beyer, H. Carl, S. Gregor, D. Lucas, H. Pietruske, P. Schütz, F. P. Schütz, *Nucl. Eng. Des.* **2007**, *237*, 1848.

[14] N. Omebere-Iyari, B. Azzopardi, D. Lucas, M. Beyer, H. M. Prasser, *Int. J. Multiphas. Flow* **2008**, *34*, 461.

[15] N. Omebere-Iyari, *Ph.D. Thesis*, University of Nottingham (Nottingham, UK) **2006**.

[16] R. Kaji, J. Hills, B. Azzopardi, *Multiphase Science and Technology* **2009**, *21*, 1.

[17] M. Abdulkadir, V. Hernandez-Perez, S. Sharaf, I. Lowndes, B. Azzopardi, *World Academy of Science, Engineering and Technology* **2010**, *61*, 52.

[18] S. Rabha, M. Schubert, U. Hampel, *AIChE J.* **2014**, *60*, 3079.

[19] A. Ibrahim, B. Hewakandamby, B. Azzopardi, presented at 10th North American Conf. on Multiphase Technology, Banff, Canada, June **2016**.

[20] G. Besagni, L. Gallazzini, F. Inzoli, *Chem. Eng. Sci.* **2018**, *176*, 116.

[21] A. Ibrahim, B. Hewakandamby, Z. Yang, B. Azzopardi, presented at ASME 5th Joint US-European Fluids Engineering Division Summer Meeting, Montreal, Canada, July **2018**.

[22] G. Besagni, F. Inzoli, T. Ziegenhein, *ChemEngineering* **2018**, *2*, 13.

[23] S. Godbole, M. Honath, Y. Shah, *Chem. Eng. Commun.* **1982**, *16*, 119.

[24] S. Mohagheghian, B. Elbing, *Fluids* **2018**, *3*, 13.

[25] S. K. Mohammed, *Ph.D. Thesis*, University of Nottingham (Nottingham, UK) **2017**.

[26] B. Azzopardi, L. Abdulkareem, D. Zhao, S. Thiele, M. J. da Silva, M. J. da Silva, A. Hunt, *Ind. Eng. Chem. Res.* **2010**, *49*, 8805.

[27] S. K. Mohammed, A. H. Hasan, G. Dimitrakis, B. Azzopardi, *Int. J. Multiphas. Flow* **2018**, *100*, 16.

[28] S. K. Mohammed, A. H. Hasan, A. Ibrahim, G. Dimitrakis, B. Azzopardi, *Int. J. Multiphas. Flow* **2019**, *120*, 103095.

[29] A. H. Hasan, S. K. Mohammed, L. Pioli, B. Hewakandamby, B. Azzopardi, *Int. J. Multiphas. Flow* **2019**, *116*, 1.

[30] J. Bird, R. De Ruiter, L. Courbin, H. Stone, *Nature* **2010**, *465*, 759.

[31] T. Kamei, A. Serizawa, *Nucl. Eng. Des.* **1998**, *184*, 349.

[32] Z. Khatib, J. Richardson, *Chem. Eng. Res. Des.* **1984**, *62*, 139.

[33] J. Q. Feng, *J. Fluid Mech.* **2008**, *609*, 377.

[34] R. Davies, G. Taylor, *P. Roy. Soc. A-Math. Phy.* **1950**, *200*, 375.

[35] D. Nicklin, *Chem. Eng. Sci.* **1962**, *17*, 693.

[36] F. Viana, R. Pardo, R. Yánez, J. L. Trallero, D. D. Joseph, *J. Fluid Mech.* **2003**, *494*, 379.

[37] B. Azzopardi, L. Pioli, L. Abdulkareem, *Int. J. Multiphas. Flow* **2014**, *67*, 160.

[38] R. Collins, F. F. De Moraes, J. Davidson, D. Harrison, *J. Fluid Mech.* **1978**, *89*, 497.

[39] A. E. Dukler, J. Fabre, *Multiphase Science and Technology* **1994**, *8*, 1.

[40] S. Guet, G. Ooms, R. V. A. Oliemans, R. Mudde, *Chem. Eng. Sci.* **2004**, *59*, 3315.

[41] M. Stewart, *Surface Production Operations: Facility Piping and Pipeline System*, Gulf Professional Publishing, Waltham, MA **2016**, p. 343.

[42] S. Mokhatab, W. A. Poe, J. G. Speight, *Handbook of Natural Gas Transmission and Processing*, 3rd ed., Gulf Professional Publishing, Boston, MA **2015**, p. 37.